Icarus 206 (2010) 112–119

Contents lists available at ScienceDirect

Icarus

journal homepage: www.elsevier.com/locate/icarus

# Localized ionization patches in the nighttime ionosphere of Mars and their electrodynamic consequences

M.O. Fillingim [a,*], L.M. Peticolas [a], R.J. Lillis [a], D.A. Brain [a], J.S. Halekas [a], D. Lummerzheim [b], S.W. Bougher [c]

[a] Space Sciences Laboratory, University of California, Berkeley, CA 94720-7450, USA
[b] Geophysical Institute, University of Alaska, Fairbanks, AK 99775-7320, USA
[c] Department of Atmospheric, Oceanic and Space Sciences, University of Michigan, Ann Arbor, MI 48109-2143, USA

ARTICLE INFO

*Article history:*
Received 25 September 2008
Revised 5 February 2009
Accepted 2 March 2009
Available online 10 March 2009

*Keywords:*
Mars, atmosphere
Ionospheres
Magnetic fields

ABSTRACT

Using an electron transport model, we calculate the electron density of the electron impact-produced nighttime ionosphere of Mars and its spatial structure. As input we use Mars Global Surveyor electron measurements, including an interval when accelerated electrons were observed. Our calculations show that regions of enhanced ionization are localized and occur near magnetic cusps. Horizontal gradients in the calculated ionospheric electron density on the night side of Mars can exceed $10^4$ cm$^{-3}$ over a distance of a few tens of km; the largest gradients produced by the model are over 600 cm$^{-3}$ km$^{-1}$. Such large gradients in the plasma density have several important consequences. These large pressure gradients will lead to localized plasma transport perpendicular to the ambient magnetic field which will generate horizontal currents and electric fields. We calculate the magnitude of these currents to be up to 10 nA/m$^2$. Additionally, transport of ionospheric plasma by neutral winds, which vary in strength and direction as a function of local time and season, can generate large (up to 1000 nA/m$^2$) and spatially structured horizontal currents where the ions are collisionally coupled to the neutral atmosphere while electrons are not. These currents may contribute to localized Joule heating. In addition, closure of the horizontal currents and electric fields may require the presence of vertical, field-aligned currents and fields which may play a role in high altitude acceleration processes.



## 1. Introduction

It is well known that Mars lacks a globally coherent magnetic field; however, it does possess intense and localized crustal magnetic fields (Acuña et al., 1998, 2001). The interaction of the crustal fields with the interplanetary magnetic field (IMF) leads to a complex magnetic topology (Mitchell et al., 2001; Brain et al., 2007). In general, in regions where the crustal fields are nearly radial, they have a tendency to connect to the IMF, forming magnetic cusps. Such cusps provide a conduit for solar wind electrons to access the night side atmosphere. Where solar wind electrons impact the night side atmosphere, they should ionize the atmospheric constituents creating a night side ionosphere. Directly above the strongest crustal magnetic sources where the fields are horizontal, solar wind electrons do not have access to the atmosphere, and there is an absence of ionization, i.e., plasma voids.

The complex magnetic topology creates a highly structured night side ionosphere. Solar wind electrons have direct access to the atmosphere in the vicinity of magnetic cusps. (Electron impact ionization can also be responsible for the formation of a nighttime ionosphere in the relatively un-magnetized northern hemisphere where solar wind electrons have access to the atmosphere along draped solar wind magnetic field lines.) The global distribution of cusps is non-uniform (Krymskii et al., 2002); therefore, the distribution of night side ionization is likewise expected to be non-uniform, i.e., "patchy." Three classes of recent observations suggest that this is in fact the case: observations of downward traveling accelerated electrons, direct observations of ionospheric structure, and observations of localized auroral emission.

Recent observations from both Mars Global Surveyor (MGS) (Brain et al., 2006; Halekas et al., 2008) and Mars Express (Lundin et al., 2006a, 2006b) have shown downward-traveling accelerated electrons. The accelerated electron spectra have relatively narrow peaks in the electron flux with peak energies from about 100 eV up to a few keV, similar in shape to accelerated electron spectra observed in Earth's auroral zone. These observations of accelerated electrons are not spatially uniformly distributed. Instead, they are often observed to be collocated with radial magnetic fields at cusps.

Data from the Mars Advanced Radar for Subsurface and Ionosphere Sounding (MARSIS) onboard Mars Express have also indicated the presence of structure in the nighttime ionosphere. Enhancements in the maximum electron density have been observed on both the dayside (Gurnett et al., 2005, 2008;

* Corresponding author. Fax: +510 643 8302.
*E-mail address:* matt@ssl.berkeley.edu (M.O. Fillingim).

0019-1035/$ - see front matter © 2009 Elsevier Inc. All rights reserved.
doi:10.1016/j.icarus.2009.03.005

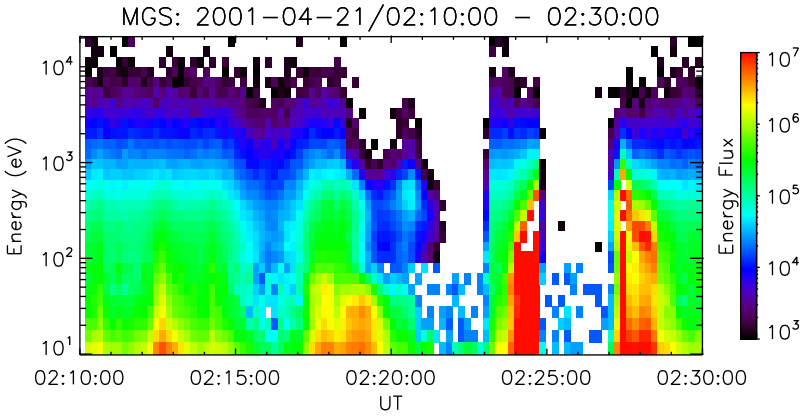


**Fig. 1.** Input electron energy spectrogram observed by Mars Global Surveyor at 02 local time on 21 April 2001 at an altitude of 400 km. During the time of observation, MGS was moving southward from −10° to −70° latitude along the 210° East longitude meridian. The spacecraft solar zenith angle varied between 100° and 120°. Two accelerated electron events are seen(at 02:24 UT and 02:28 UT) in cusp regions; an interval of very little electron flux separates them – a plasma void.

Duru et al., 2006) and nightside (Kirchner et al., 2006, 2007). The short time duration and the shape of the radar echoes reflecting off of the high density structures indicate that the regions of enhanced density typically have scale sizes of a few tens of km (Duru et al., 2006). In addition, MARSIS measurements have shown localized increases of the ionospheric total electron content (TEC) on both the dayside and nightside that are generally correlated with vertical magnetic fields in cusp regions (Safaeinili et al., 2007; Mouginot et al., 2008).

Finally, Bertaux et al. (2005) reported the first observations of auroral emission at Mars from Mars Express. These and subsequent observations (Leblanc et al., 2008) showed that auroral emission is localized and also occurs in the vicinity of magnetic cusps. Leblanc et al. (2008) showed simultaneous observations of auroral-type emissions, precipitating energetic electrons, and increases in the ionospheric TEC. These observations suggest that these phenomena are related leading to a consistent picture with the precipitating electrons causing the enhanced ionization and auroral emission.

Previously, Haider et al. (1992) and Fox et al. (1993) calculated the expected ionospheric density from two different electron spectra observed by Phobos-2: one from the magnetotail lobe and one from the plasma sheet. Both authors found that the plasma sheet spectrum increased the ionospheric density by about 40% over that due to the lobe spectrum. However, due to the high altitude of the observations (~10,000 km), it was undetermined whether the electrons would in fact impact the atmosphere.

Recently, Fillingim et al. (2007) modeled the change in the ionospheric density using low altitude (400 km) MGS electron observations. As input to their model, they used an accelerated electron spectrum observed in a magnetic cusp and a typical nightside electron spectrum measured only a few minutes apart. The maximum electron density and TEC produced by the accelerated electrons were calculated to be about a factor of 3 higher than that due to the typical tail spectrum. Here we extend this earlier work by using a larger sample of observed electron spectra as input (a total of 100) in order to calculate the horizontal gradients in the ionospheric density. These density gradients are expected to play an important role in ionospheric electrodynamics. Strong gradients in the electron density will lead to strong gradients in the horizontal ionospheric currents which may in turn lead to structure in the electric fields and field-aligned currents.

## 2. Methodology

To model the electron transport in the Martian atmosphere, we use a modification of the code of Lummerzheim and Lilensten (1994) developed to model electron transport in the auroral ionosphere of Earth. This code uses the discrete-ordinate method to solve the energy degradation and electron transport problem and uses a multi-stream approach to solve for the electron flux as a function of energy and altitude.

Necessary modifications to the model of Lummerzheim and Lilensten (1994) include incorporating the appropriate CO and $CO_2$ cross sections for electron impact and using a Martian atmospheric neutral density profile. Currently, the code incorporates over 100 types of elastic and inelastic collisions including dissociations, excitations, and ionizations using cross sections compiled by Lummerzheim and Lilensten (1994) for O, $O_2$, and $N_2$, and by J. Fox and K. Sung (2001, personal communication), Liu and Victor (1994), and Itikawa (2002) for CO and $CO_2$.

The neutral atmosphere is given by the Mars Thermospheric Global Circulation Model (MTGCM) (Bougher et al., 1999, 2000, 2006; McDunn et al., 2008). The number densities of $CO_2$, CO, $O_2$, O, $N_2$, and Ar are given from 100 to 250 km altitude (however, Ar is not included in the electron transport calculations). Below 100 km, the density is extrapolated logarithmically and the temperature is extrapolated linearly. Above 250 km, the density is extrapolated assuming diffusive equilibrium and an isothermal profile ($T$ = 163 K in this case). The profile used here is from 2.5° north latitude at a local time of 3 AM under solar medium conditions at equinox. However, the exact choice of seasonal and geographic parameters is not of critical importance since our goal is to determine the change in the ionospheric density due to different incident spectra.

The input electron spectrogram is shown in Fig. 1. These data were observed by MGS on 21 April 2001 and have been reported in more detail by Brain et al. (2006). From 02:10 to 02:30 UT, MGS was at an altitude of about nearly 400 km at a local time of 02 on the night side. During this interval, the spacecraft moved from about −10° to −70° latitude along the 210° east meridian while the spacecraft's solar zenith angle varied between 150° to 120°. Significant variations in the electron energy flux are seen over this interval; two accelerated electron events are seen – one near 02:24 UT and another at 02:28 UT – in cusp regions on either side of a plasma void. A second plasma void is centered at 02:22 UT.

The electron transport model does not include gradients in the magnetic field. The magnetic field lines are assumed to be straight with a constant dip angle and magnitude. However, at each observations point, the path length of the electrons through the atmosphere is adjusted by changing the dip angle of the magnetic field to match the dip angle given by the crustal magnetic field

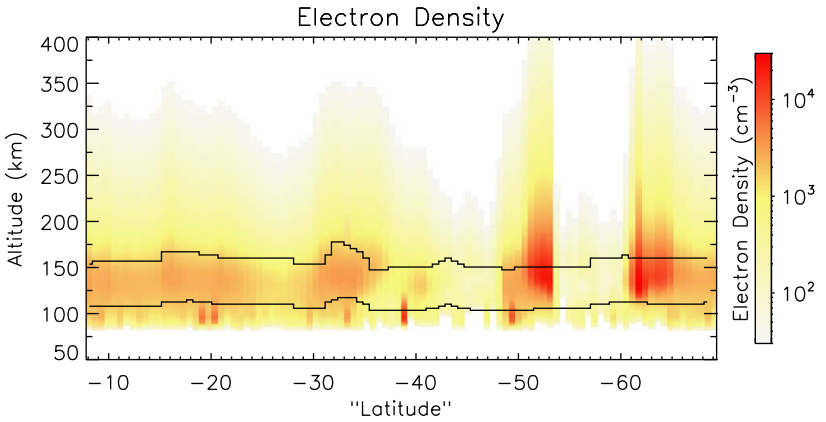


**Fig. 2.** Calculated electron density as a function of altitude and "latitude." The altitude where ω/ν = 1 for both the ions (lower line) and electrons (upper line) is also shown. Above this line, charged particles are magnetized; below this line, they are collisional. The *X*-axis shows the latitude of the spacecraft observation rather than the latitude where the magnetic field intersects the surface. Each column represents the electron density along an assumed straight magnetic field line from an altitude of 400 km down to 50 km. The highest peak electron densities occur in cusps where the input electron energy flux is highest. The lowest peak electron densities occur in the plasma voids.

model of Cain et al. (2003) near 150 km. Throughout this interval, the dip angle at 150 km ranges between 50° and 90° from the horizontal with an average dip angle of 70°.

## 3. Results

Using the observed electron spectrogram as an upper boundary condition, the ion production rates due to electron impact ionization can be calculated. A vertical ion production rate profile is computed for each input electron spectrum shown in Fig. 1 (100 total). The peak ion production rate varies by five orders of magnitude from 0.003 $cm^{-3}$ $s^{-1}$ in a void to 300 $cm^{-3}$ $s^{-1}$ due to an accelerated spectrum in a cusp. The mean and median peak production rates over the entire interval are 13 and 1.9 $cm^{-3}$ $s^{-1}$, respectively.

Our calculated maximum and minimum peak production rates bracket those previously computed by Haider et al. (1992) and Fox et al. (1993) using high altitude Phobos 2 electron observations as input. Their computed peak production rates due to the magnetotail lobe spectrum were 30 and 20 $cm^{-3}$ $s^{-1}$, respectively; the peak production rates due to the plasma sheet spectrum were 65 and 52 $cm^{-3}$ $s^{-1}$, respectively. Later, using a precipitating solar wind electron spectrum observed by MGS, Haider et al. (2002) computed a peak ion production rate of 6 $cm^{-3}$ $s^{-1}$. [Our average peak production rates agree well with those computed by Haider et al. (1992) and Fox et al. (1993) due to the lobe spectrum. Our median (typical) peak production rate is significantly lower that the rates computed by Haider et al. (1992) or Fox et al. (1993) for either the lobe or plasma sheet spectra. However, as noted in Fillingim et al. (2007), the electron fluxes below 300 eV used by Haider et al. (1992) and Fox et al. (1993) were up to an order of magnitude larger than those used by Fillingim et al. (2007). Likewise, the median electron spectrum from the interval used here has a much lower flux at energies below 300 eV than the spectra used by Haider et al. (1992) and Fox et al. (1993).]

The ionospheric electron number density can be computed from the total ion production rate (ignoring dynamics and assuming photochemical equilibrium) from the equation

$$n_e(z) = (P(z)/\alpha_{\mathrm{eff}}(z))^{1/2}\mathrm{cm}^{-3},$$

where $P(z)$ is the ion production rate and $\alpha_{\mathrm{eff}}$ $(z)$ is the effective recombination rate. Due to rapid chemical reactions between $CO_2$, O, and their ions, $O_2^+$ is the dominant ion in the ionosphere of Mars over the altitudes considered here (Fox et al. 1993, 1996; Haider 1997). Therefore, $\alpha_{\mathrm{eff}}$ $(z)$ is taken to be the dissociative recombination rate of $O_2^+$ (e.g., Sheehan and St.-Maurice, 2004):

$$\alpha_{\mathrm{eff}}(z) = 1.95 \times 10^{-7}(300/T_e(z))^{0.7}\mathrm{cm}^3\mathrm{s}^{-1},$$

where $T_e$ is the electron temperature. In the absence of electron temperature observations on the night side, we assume that the electron temperature is equal to the neutral temperature. At low altitudes (~100 km), the neutral temperature given by the MTGCM is about 110 K. Above 150 km, the temperature is about 160 K. While this may be a somewhat reasonable assumption at low altitudes, this is most likely a significant underestimate of the electron temperature, thus an underestimate of the electron density, at high altitude. Below, we will discuss the changes in the electron number density resulting from using a different electron temperature profile.

The computed electron density as a function of altitude and "latitude" is shown in Fig. 2. The latitude shown on the *X*-axis is the latitude of the spacecraft observation rather than the latitude where the magnetic field lines intersect the surface. Rather than a true two-dimensional representation of the ionosphere where there can be significant curvature in the magnetic field, each vertical column in Fig. 2 represents the electron density along an assumed straight magnetic field line from an altitude of 400 km.

These calculations show that the maximum peak electron densities have magnitudes of $\sim 3 \times 10^4$ $cm^{-3}$ at altitudes of ~140 km and occur in the cusps where the input electron energy flux is highest. Maximum TEC also occur in these same regions and have values of $\sim 1.4 \times 10^{15}$ $m^{-2}$ or 0.14 TEC units (1 TECU is equal to $10^{16}$ $m^{-2}$). These values are greater than 10% of the peak subsolar dayside values of $\sim 2 \times 10^5$ $cm^{-3}$and $\sim 1 \times 10^{16}$ $m^{-2}$ (e.g., Mendillo et al., 2004; Safaeinili et al., 2007; Mouginot et al., 2008). In a plasma void, the calculated minimum peak electron densities are $\sim 1 \times 10^2$ $cm^{-3}$ and occur at slightly lower altitudes near 100 km. The minimum TEC in a void is calculated to be $\sim 7.3 \times 10^{12}$ $m^{-2}$ or $7.3 \times 10^{-4}$ TECU. The average peak electron density and median peak electron density over this interval are $3.8 \times 10^3$ $cm^{-3}$ and $2.5 \times 10^3$ $cm^{-3}$, respectively. The average and median TEC are $2.1 \times 10^{14}$ and $1.8 \times 10^{14}$ $m^{-2}$, respectively. (We should note that due to refinements in the energy grid of the electron transport model, the electron density values reported here are about 2.5 times higher than those reported in Fillingim et al., 2007.)

Again, these calculated electron densities bracket those computed previously (Haider et al., 1992; Fox et al., 1993; Haider et al., 2002). Our calculations also compare well with measurements of the nightside ionosphere. Kirchner et al. (2006, 2007) have

reported nightside ionospheric densities measured by MARSIS to range from less than $2 \times 10^3$ cm$^{-3}$ to typical values of $8 \times 10^3$ cm$^{-3}$ over non-magnetic regions. Over magnetized regions in the southern hemisphere, the nightside ionospheric density is observed to typically be $5 \times 10^4$ cm$^{-3}$ with an absolute maximum of $1.8 \times 10^5$ cm$^{-3}$ measured so far. Our computed maximum peak electron density of $3 \times 10^4$ cm$^{-3}$ is in relatively good agreement with the typical peak density of $5 \times 10^4$ cm$^{-3}$ as observed by MARSIS in magnetized regions (Kirchner et al., 2007). Additionally, Safaeinili et al. (2007) reported nightside TEC values measured by MARSIS to vary from less than $10^{13}$ m$^{-2}$ up to nearly $10^{15}$ m$^{-2}$ with typical values on the order of $10^{14}$ m$^{-2}$ or less. Our computed maximum ($1.4 \times 10^{15}$ m$^{-2}$), minimum ($7.3 \times 10^{12}$ m$^{-2}$), and average ($2 \times 10^{14}$ m$^{-2}$) values of TEC compare quite well with the MARSIS observations.

Also shown in Fig. 2 are the altitudes at which the collision frequency, $\nu$, equals the gyro-frequency, $\omega$, for the ions (upper line) and for the electrons (lower line). Above these altitudes, magnetic effects dominate the particle dynamics; below these altitudes, collisions dominate the dynamics. This transition occurs at about 160 km for ions and at about 110 km for electrons. The altitude depends upon the neutral density as well as the magnetic field magnitude (and for the electrons, the electron temperature). In the region between these two altitudes, the ions are collisionally coupled to the atmosphere while the electrons are still magnetized. The ions will move in the direction of an applied force (e.g., pressure gradients or neutral winds); the electrons, in contrast, will move perpendicular to both an applied force and the magnetic field. This is the so-called ionospheric dynamo region.

From Fig. 2, it is clear that throughout the interval the altitude of the dynamo region coincides with the peak in ionospheric density. The current density, **j**, is given by

$$\mathbf{j} = nq(\mathbf{v}i - \mathbf{v}e).$$

Since the plasma density, $n$, and the difference between the ion and electron velocities, ($\mathbf{v_i} - \mathbf{v_e}$), are both largest in this dynamo region, horizontal ionospheric currents should also be largest in this region. In the following section, the horizontal ionospheric currents are computed for three limiting cases: latitudinal pressure gradient, uniform latitudinal (northward) neutral wind, and uniform longitudinal (westward) neutral wind.

To determine ionospheric currents, we start with a simplified momentum equation assuming steady state conditions and all forces in equilibrium. In this derivation, we only consider non-resonant collisions between the charged particles (ions and electrons) and atmospheric neutrals. We neglect Coulomb collisions, i.e., ion-ion and ion–electron collisions. Ion–electron collisions couple the electron dynamics to the ion motion and can be important under certain circumstances; however, they do not significantly affect the currents at the altitude of the ionospheric peak (e.g., Heelis et al., 1985). During this interval, the typical electron–ion collision frequency exceeds the electron neutral collision frequency at an altitude of ~160 km. At this altitude, the electrons will respond more to ion motions than to neutral motions. However, at this altitude, the electrons are already strongly magnetized, so collisional effects will be small. At other regions on Mars where the magnetic field can be much weaker, including electron–ion collisions is essential to describing the electron motion.

With the above assumptions in mind, the ion and electron equations of motion are

ions:

$$-\frac{1}{n_i}\nabla(n_i k T_i) + m_i\mathbf{g} + q(\mathbf{E} + \mathbf{v}_i \times \mathbf{B}) - m_i \nu_{\mathrm{in}}(\mathbf{v}_i - \mathbf{u}) = 0$$

electrons:

$$-\frac{1}{n_e}\nabla(n_e k T_e) + m_e\mathbf{g} - q(\mathbf{E} + \mathbf{v}_e \times \mathbf{B}) - m_e \nu_{\mathrm{en}}(\mathbf{v}_e - \mathbf{u}) = 0$$

First, we only consider the latitudinal pressure gradient. In this highly idealized case, we assume that the pressure gradient is only in the $X$-direction (latitudinal). Additionally, the effects of gravity, **g**, the electric field, **E**, and the neutral wind velocity, **u**, are ignored. Also, we further simplify the problem by assuming that the magnetic field is only in the $Z$-direction, i.e., $\mathbf{B} = B_Z$. This final simplification is, of course, unphysical since the dip angle varies between 50° and 90° over this region according to the model of Cain et al. (2003). We make this simplification so that the particle velocities and currents can be expressed analytically and to enhance the physical understanding of the processes giving rise to the currents. In actuality, non-vertical magnetic fields will lead to vertical transport of the plasma which will modify the altitude and height distribution of the ionized layer. With these assumptions, solving for the ion and electron velocities gives

$$v_{\mathrm{ix}} = -\frac{1}{n_i}\frac{d(n_i k T_i)}{dx}\frac{\nu_{\mathrm{in}}}{m_i}\frac{1}{(\omega_i^2 + \nu_{\mathrm{in}}^2)},$$
$$v_{\mathrm{iy}} = -\frac{\omega_i}{\nu_{\mathrm{in}}}v_{\mathrm{ix}},$$
$$v_{\mathrm{ex}} = -\frac{1}{n_e}\frac{d(n_e k T_e)}{dx}\frac{\nu_{\mathrm{en}}}{m_e}\frac{1}{(\omega_e^2 + \nu_{\mathrm{en}}^2)},$$
$$v_{\mathrm{ey}} = \frac{\omega_e}{\nu_{\mathrm{en}}}v_{\mathrm{ex}}.$$

Once the ion and electron velocities are determined, the latitudinal ($X$-component) and longitudinal ($Y$-component) current densities can be computed from the current density equation.

Fig. 3 shows the $X$- and $Y$-components of the current density due to the latitudinal plasma pressure gradient. The currents are relatively weak and highly localized in latitude and altitude. The largest pressure gradients occur at cusp–void interfaces; not surprisingly, the largest currents are found in these regions. Latitudinal currents (positive northward) flow toward low density voids and outward from high density cusps. The latitudinal currents are analogous to Pedersen currents in that they flow in the direction of the applied force (the plasma pressure gradient) and depend upon the ratio $\nu/(\omega^2 + \nu^2)$. Longitudinal currents – Hall-like in that they flow perpendicular to the applied force and depend upon the ratio $\omega/(\omega^2 + \nu^2)$ – flow along cusp boundaries.

Next, we compute the horizontal ionospheric currents due to a uniform latitudinal neutral wind; $u_x$ is set to 100 m/s northward at all latitudes and altitudes. This is a gross simplification of the actual neutral wind structure chosen to illustrate the neutral wind effect on the ionospheric currents. However, MTGCM calculations by Bougher et al., (1999), Bougher et al. (2000) have shown that relatively uniform northward neutral winds with speeds up to a few 100 m/s can occur on the nightside in the southern hemisphere particularly near equinox and southern summer solstice. The ion and electron velocities for this case are

$$v_{\mathrm{ix}} = m_i \nu_{\mathrm{in}} u_x \frac{\nu_{\mathrm{in}}}{m_i}\frac{1}{(\omega_i^2 + \nu_{\mathrm{in}}^2)} = \frac{\nu_{\mathrm{in}}^2}{(\omega_i^2 + \nu_{\mathrm{in}}^2)}u_x,$$
$$v_{\mathrm{iy}} = -\frac{\omega_i}{\nu_{\mathrm{in}}}v_{\mathrm{ix}},$$
$$v_{\mathrm{ex}} = m_e \nu_{\mathrm{en}} u_x \frac{\nu_{\mathrm{en}}}{m_e}\frac{1}{(\omega_e^2 + \nu_{\mathrm{en}}^2)} = \frac{\nu_{\mathrm{en}}^2}{(\omega_e^2 + \nu_{\mathrm{en}}^2)}u_x,$$
$$v_{\mathrm{ey}} = \frac{\omega_e}{\nu_{\mathrm{en}}}v_{\mathrm{ex}}.$$

The resulting currents are shown in Fig. 4. In high density regions (in this case, two cusps on either side of a void), ion drag from the northward neutral wind leads to large northward currents. These currents are up to 100 times larger than currents due to the pressure gradient.

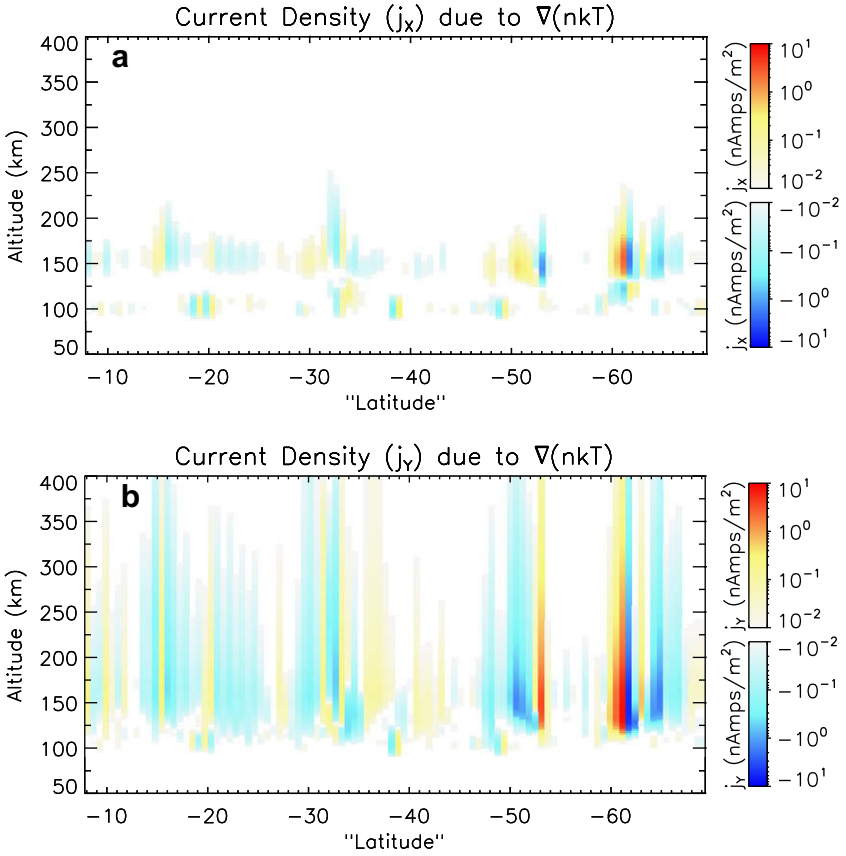


**Fig. 3.** Calculated *X*- (top) and *Y*-components (bottom) of the current density due to the latitudinal plasma pressure gradient. Pedersen-type currents (parallel to the direction of the applied force) flow in the *X*-direction; Hall-type currents (perpendicular to both the applied force and the magnetic field) flow in the *Y*-direction. In the top (bottom) panels, shades of red indicate northward (westward) currents, while shades of blue indicate southward (eastward) currents.(For interpretation of the references to color in this figure legend, the reader is referred to the web version of this article.).

In these same regions, longitudinal (Hall-like) currents flow as electrons drift in the $-\mathbf{F} \times \mathbf{B}$ direction where $\mathbf{F} = F_X = mv_{en}u_X$. Since the direction of the magnetic field on each side of the void changes direction, the longitudinal current on each side of the void also changes direction, being directed eastward (negative) near $-50°$ latitude and westward (positive) more poleward near $-60°$.

In the third and final case, the driving force is a uniform longitudinal neutral wind, $u_Y$, which is set to 100 m/s westward at all latitudes and altitudes. Again, this is a simplification of the actual neutral winds, but Bougher et al. (2000) have shown that a relatively uniform eastward neutral wind pattern can occur on the nightside in the southern hemisphere near northern summer solstice. In this case, the *Y*-components of the ions and electron velocities are equal to the *X*-components given above for the second case; the *X*-components of the velocities are equal to the negative of the *Y*-components given above. The resulting horizontal currents are shown in Fig. 5.

The *Y*-component of the current is identical to the *X*-component shown in Fig. 4. This current is due to ion drag in the direction of the neutral wind flow (in the positive *Y*-direction). The latitudinal (Hall-like) currents now flow outward latitudinally away from the void (however, if the direction of the neutral wind is reversed, i.e., eastward rather than westward, the currents would flow inward latitudinally into the void).

## 4. Discussion

By comparing the results of these cases, it is clear that, in the complex topology of the crustal fields, the direction of the neutral winds has a profound effect on the direction and magnitude of the horizontal ionospheric currents. The ion-drag current flows in the direction of the neutral wind flow. The direction of the perpendicular, Hall-like current carried by the electrons depends upon the orientation of the magnetic field which can change on spatial scales smaller than 100 km at ionospheric altitudes.

This small scale structure in the magnetic field will create small scale spatial structure in the currents. Small scale structure in the magnitude of the magnetic field affects the ratio of the gyro-frequency to the collision frequency, $\omega/\nu$, and changes the altitude at which the ions and electrons transition from being collisionally coupled to the atmosphere to being strongly magnetized. This ratio appears in the expressions for the particle velocities, hence the current density equation. Therefore, enhanced electron precipitation is not necessary for small scale spatial structure to exist in the horizontal currents. However, in the absence of enhanced ionization, the magnitude of the currents will be relatively small even though significant structure may exist. The effect of enhanced electron precipitation is to create even smaller scale structure–a few 10s of km–in the horizontal ionospheric current patterns since the regions of enhanced precipitation are of this size.

On the dayside, where solar ionizing radiation produces a much smoother latitudinal profile in the electron density, strong currents will still exist in the dynamo region in the presence of neutral winds due to the large electron densities. Horizontal gradients in the current will be smaller because of the lack of latitudinal structure in the electron density. However, structure will still exist in the ionospheric currents due to small scale structure in the magnitude and orientation of the magnetic field.

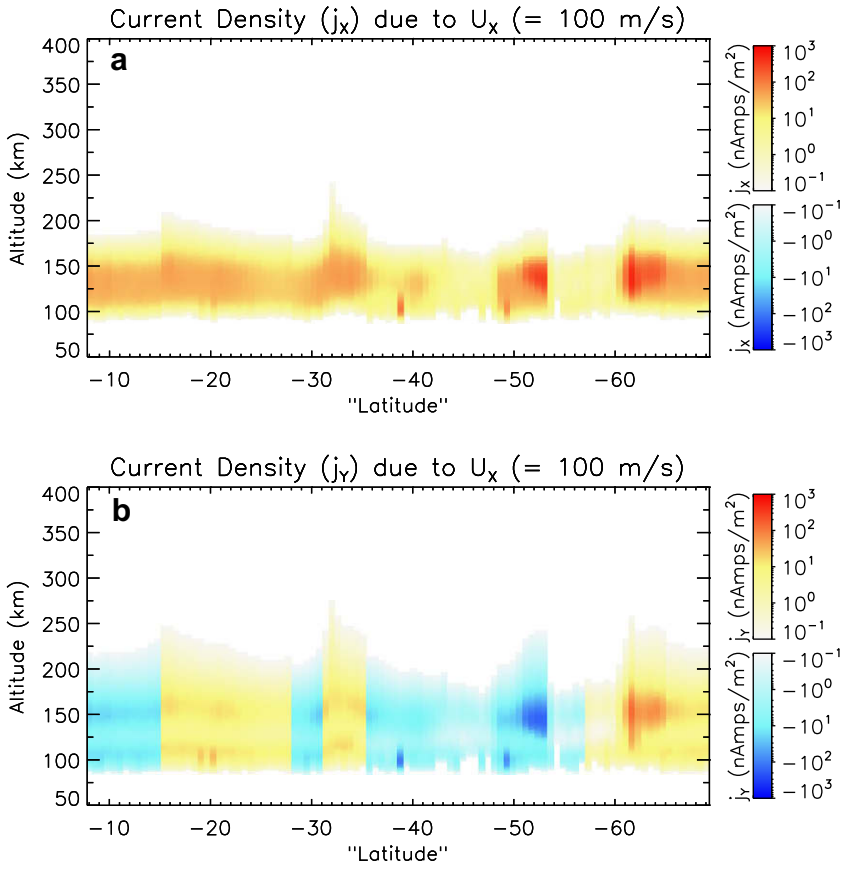


**Fig. 4.** Same as Fig. 3 except due to a 100 m/s northward neutral wind uniform in latitude and altitude. Abrupt changes in the direction of the *Y*-component of the current are due to changes in the direction of the magnetic field.

If the divergence of the horizontal currents is non-zero, then field-aligned currents are needed for current closure. In the nighttime ionosphere, the ambient plasma density may not be sufficient to carry the required current. If this is the case, a potential drop can form above the ionosphere to accelerate the plasma, i.e., the potential increases the plasma velocity, **v**, in the current density equation since the plasma density, *n*, is limited. Such is often the case in Earth's auroral ionosphere (Newell et al., 2001). Therefore the divergence of horizontal currents can lead to high altitude acceleration processes which may be related to recent observations of accelerated electrons (Brain et al., 2006; Lundin et al., 2006a, 2006b; Halekas et al., 2008).

The modeling and computations shown here are an over-simplification of the real electrodynamics of the nighttime Martian ionosphere. When interpreting these results, there are several caveats to keep in mind. First, we use a single atmospheric profile taken from the MTCGM at 2.5° N latitude. In actuality, the input data observed by MGS spans 50° of latitude. The neutral density and temperature profiles as well as the wind fields will change over this broad latitude range. In this work, for simplicity, we have neglected these changes. A more realistic assessment of the ionospheric currents will require a more realistic representation of the neutral density, temperature and winds as a function of latitude.

Due to a lack of measured electron temperatures in the nighttime atmosphere, we have also made the assumption that the electron temperature is equal to the neutral temperature. This may be a reasonable assumption in the collisional regime (up to ~ 100 km); however, this assumption leads to an underestimate of the electron temperature at higher altitude. This will in turn lead to an underestimate of the electron density at high altitude since the effective recombination rate is dependent upon electron temperature. To quantify this effect, we recomputed the electron density profiles using an electron temperature equal to that derived from the in situ Viking lander observations on the dayside (Hanson et al., 1977) as an upper limit to the nightside electron temperature. Specifically, we used the dayside electron temperature of Fox (1993) which fits the data to two exponential functions:

$$T_e = T_n; \quad z < 130\text{km}$$
$$T_e = 700 - 536\exp[(130 - z)/65.4]; \quad 130 < z < 180\text{km}$$
$$T_e = 4200 - 3750\exp[(180 - z)/89.6]; \quad z > 180\text{km}$$

Using these higher electron temperature values, the peak ionospheric electron densities increase by about 15%. This relatively small increase is due to the fact that the calculated peak electron densities occur near altitudes of 140 km before the electron and neutral temperatures have diverged much. The higher electron temperature also has the effect of raising the altitude of the peak by 3 to 4 km. The TEC, in contrast, increases by about 30% when computed using the higher electron temperature. Since the dayside electron temperature rises exponentially, the electron density at high altitude is greatly enhanced over that computed assuming the electron temperature is equal to the neutral temperature. The higher electron density at high altitude leads to a larger increase in TEC than for the peak electron densities.

The electron–neutral collision frequency, $\nu_{en}$, also depends upon the electron temperature, so it is expected that the collision frequencies are also underestimated at high altitudes when assuming that the electron temperature is equal to the neutral temperature. Since the electron collision frequency enters the current density equation through the electron velocity, this underestimate also affects the horizontal current calculations. Again, we recomputed the horizontal ionospheric currents assuming the nightside

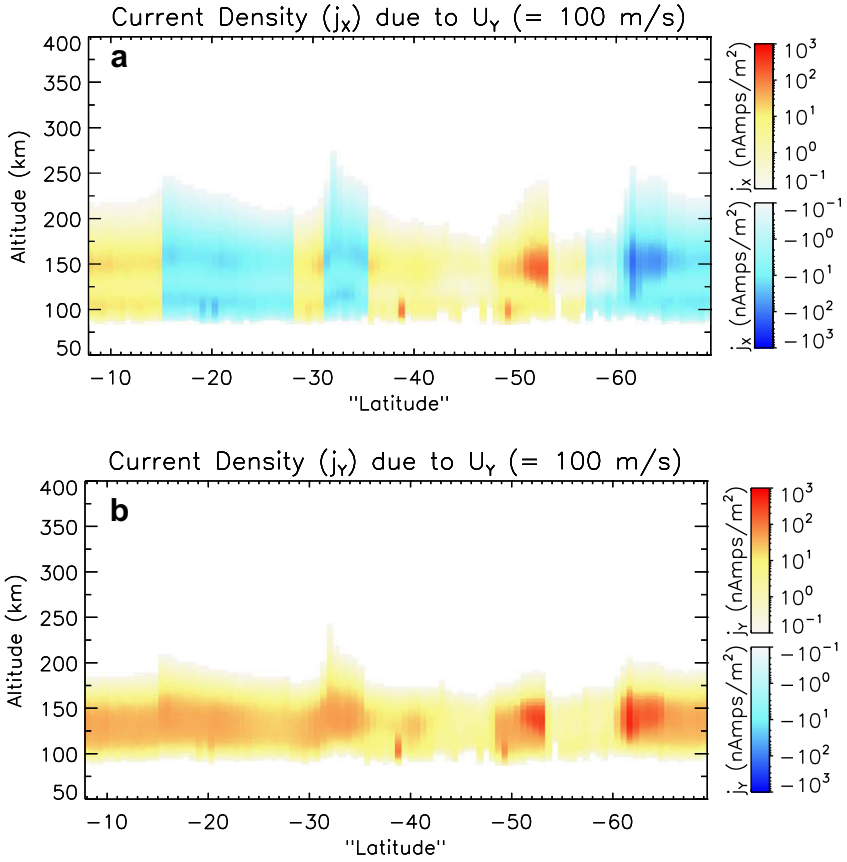


**Fig. 5.** Same as Fig. 3 except due to a 100 m/s westward neutral wind uniform in latitude and altitude.

electron temperature is equal to the dayside electron temperature to quantify the effect of changing electron temperature on current magnitude. The Pedersen-type currents (the latitudinal currents in cases 1 and 2 above and the longitudinal current in case 3) are carried by the ions in the dynamo region. Since the ion velocities are not affected by the increased electron temperature, the change in the peak Pedersen-type currents is about 15%, equal to the increase in the peak electron densities as expected from the current density expression. (In actuality, as shown by Hanson et al. (1977) and Fox et al. (1993), the dayside ion temperature begins to deviate from the neutral temperature at nearly 200 km altitude approaching the dayside electron temperature at about 300 km altitude. However, the ion densities and the ion-neutral collision frequencies are too low at these altitudes for the currents to be significantly affected.) The peak Hall-type currents, which are carried mostly by the electrons, increase by nearly 30%. This is because not only does the peak electron density increase, but also the electron-neutral collision frequency which, in turn, affects the electron velocity. When $\omega_e > \nu_{en}$, small increases in $\nu_{en}$ lead to increases in the electron velocity in the $-\mathbf{F} \times \mathbf{B}$ direction.

Currently, the electron transport model does not include gradients in the magnetic field. Magnetic field lines are assumed to be straight with a constant dip angle and magnitude. At Mars, where the scale length of changes in the magnetic field can be relatively small, this is a poor assumption. We try to minimize the impact of this assumption by choosing a dip angle of the magnetic field that matches the dip angle given by the crustal magnetic field model of Cain et al. (2003) near 150 km, the altitude of greatest ionization. Strong magnetic gradients can reflect a significant portion of the downward-travelling electrons. However, if the downgoing spectrum is isotropic, the electron flux remains constant with altitude because loss of electrons by magnetic reflection is balanced by the decrease in area of the flux tube through which the electrons travel; only the area upon which the electrons precipitate will decrease. Brain et al. (2006) showed that throughout most of this interval, electron pitch angles observed by MGS were approximately isotropic so the effects of neglecting magnetic gradients should be minimal.

When calculating the horizontal ionospheric currents, for analytical simplicity, we assume that the magnetic field is vertical, i.e., $\mathbf{B} = B_Z$. Given the small scale structure of the magnetic field, this is also a poor assumption. This assumption was made in order to focus on horizontal currents in the ionosphere. An *X*- or *Y*- component of the magnetic field will result in a *Z*-component (vertical) of the current density. The next step in this work is to use realistic magnetic field profiles in order to compute more realistic currents, particularly in the vertical direction.

Finally, even though we have estimated the nighttime horizontal ionospheric currents, we have not self-consistently considered the effects of these currents. The currents themselves will perturb the ambient magnetic field. Withers et al. (2005) estimated that the magnetic field due to ionospheric currents could be 40% of the ambient magnetic field. In addition, these currents will also most likely create polarization electric fields, which can in turn drive polarization currents. Also, as mentioned above, a non-zero divergence of the horizontal currents will lead to field-aligned currents. All of these effects have been ignored in this work. Since the presence of our computed ionospheric currents will change the electric and magnetic topology, the effects of the currents must be included self-consistently to accurately describe the ionospheric electrodynamics. Currently, a three-dimensional, electromagnetically self-consistent model is under development. This model will

be able to accommodate many of the short-comings cited above including a more realistic representation of the neutral densities, temperatures, and winds as a function of latitude, longitude, and altitude, the effects of magnetic gradients and curved magnetic fields, and the electrodynamic consequences of the generated currents on the ambient magnetic fields.

## 5. Conclusion

This work is a first attempt to compute the horizontal currents in the nighttime ionosphere of Mars. Using MGS data as input to an electron transport model, we calculate the resulting ionospheric density and structure. We compute horizontal ionospheric currents using the plasma pressure gradient and two different assumed neutral wind profiles as the applied driving forces. Our main result is that significant currents can exist in the ionosphere at altitudes of peak ionization where ions are collisionally coupled to the atmosphere while the electrons are not. Small scale latitudinal structure in the magnetic field and ionospheric density lead to small scale structure and sharp gradients in the current densities. Closure of the horizontal currents may require the presence of field-aligned currents which can play a role in high altitude acceleration processes. It is essential to self-consistently include the electrodynamic effects of these currents in order to accurately describe the ionospheric dynamics at Mars.

## Acknowledgments

The Mars Global Surveyor Magnetometer/Electron Reflectometer data are courtesy of Dr. Mario Acuña. The work at UCB was supported in part by NASA grant NNX06AD97G. SWB was supported by NASA grant NNG04GJ94G.

## References

Acuña, M. H., and 19 colleagues 1998. Magnetic field and plasma observations at Mars: Initial results of the Mars Global Surveyor mission. Science 279, 1676–1680.

Acuña, M. H., and 13 colleagues, 2001. Magnetic field of Mars: Summary of results from the aerobraking and mapping orbits. J. Geophys. Res. 106(23), 403–423.

Brain, D.A., Halekas, J.S., Peticolas, L.M., Lin, R.P., Luhmann, J.G., Mitchell, D.L., Delory, G.T., Bougher, S.W., Acuña, M.H., Rème, H., 2006. On the origin of aurorae on Mars. Geophys. Res. Lett. 33, L01201.

Brain, D.A., Lillis, R.J., Mitchell, D.L., Halekas, J.S., Lin, R.P., 2007. Electron pitch angle distributions as indicators of magnetic field topology near Mars. J. Geophys. Res. 112, A09201.

Bertaux, J.-L., Leblanc, F., Witasse, O., Quemerais, E., Lilensten, J., Stearn, S.A., Sandel, B., Koralev, O., 2005. Discovery of an aurora on Mars. Nature 435, 790–794.

Bougher, S.W., Engel, S., Roble, R.G., Foster, B., 1999. Comparative terrestrial planet thermospheres 2. Solar cycle variation of global structure and winds at equinox. J. Geophys. Res. 104, 16591–16611.

Bougher, S.W., Engel, S., Roble, R.G., Foster, B., 2000. Comparative terrestrial planet thermospheres 3. Solar cycle variation of global structure and winds at solstices. J. Geophys. Res. 105, 17669–17692.

Bougher, S.W., Murphy, J.R., Bell, J.M., Lopez-Valverde, M.A., Withers, P.G., 2006. Polar warming in the Mars lower thermosphere: Seasonal variations owing to changing insolation and dust distributions. Geophys. Res. Lett. 33, L02203.

Cain, J.C., Ferguson, B.B., Mozzoni, D., 2003. An $n = 90$ internal potential function of the Martian crustal magnetic field. J. Geophys. Res. 108, 5008.

Duru, F., Gurnett, D.A., Averkamp, T.F., Kirchner, D.L., Huff, R.L., Persoon, A.M., Plaut, J.J., Picardi, G., 2006. Magnetically controlled structures in the ionosphere of Mars. J. Geophys. Res. 111, A12204.

Fillingim, M.O., Peticolas, L.M., Lillis, R.J., Brain, D.A., Halekas, J.S., Mitchell, D.L., Lin, R.P., Lummerzheim, D., Bougher, S.W., Kirchner, D.L., 2007. Model calculations of electron precipitation induced ionization patches on the nightside of Mars. Geophys. Res. Lett. 34, L12101.

Fox, J.L., 1993. The production and escape of nitrogen atoms on Mars. J. Geophys. Res. 98, 3297–3310.

Fox, J.L., Brannon, J.F., Porter, H.S., 1993. Upper limits to the nightside ionosphere of Mars. Geophys. Res. Lett. 20, 1339–1342.

Fox, J.L., Zhou, P., Bougher, S.W., 1996. The Martian thermosphere/ionosphere at high and low solar activities. Adv. Space Res. 17, 203–218.

Gurnett, D.A., Kirchner, D.L., Huff, R.L., Morgan, D.D., Persoon, A.M., Averkamp, T.F., Duru, F., Nielsen, E., Safaeinili, A., Plaut, J.J., Picardi, G., 2005. Radar Soundings of the Ionosphere of Mars. Science 310, 1929–1933.

Gurrnett, D.A., and 12 colleagues, 2008. An overview of radar soundings of the Martian ionosphere from the Mars Express spacecraft. Adv. Space Res. 41, 1335-1346.

Haider, S.A., 1997. Chemistry on the nightside ionosphere of Mars. J. Geophys. Res. 102, 407–416.

Haider, S.A., Kim, J., Nagy, A.F., Keller, C.N., Verigin, M.I., Gringauz, K.I., Shutte, N.M., Szego, K., Kiraly, P., 1992. Calculated ionization rates, ion densities, and airglow emission rates due to precipitating electrons in the nightside ionosphere of Mars. J. Geophys. Res. 97, 10637–10641.

Haider, S.A., Seth, S.P., Kallio, E., Oyama, K.I., 2002. Solar EUV and electron-proton-hydrogen atom-produced ionosphere on Mars: Comparative studies of particle fluxes and ion production rates due to different processes. Icarus 159, 18–30.

Halekas, J.S., Brain, D.A., Lin, R.P., Luhmann, J.G., Mitchell, D.L., 2008. Distribution and variability of accelerated electrons at Mars. Adv. Space Res. 41, 1347–1352.

Hanson, W.B., Sanatani, S., Zuccaro, D.R., 1977. The Martian ionosphere as observed by the Viking retarding potential analyzers. J. Geophys. Res. 82, 4351–4363.

Heelis, R.A., Vickrey, J.F., Walker, N.B., 1985. Electrical coupling effects on the temporal evolution of F-layer plasma structure. J. Geophys. Res. 90, 437–445.

Itikawa, Y., 2002. Cross sections for electron collisions with carbon dioxide. J. Phys. Chem. Ref. Data 31, 749–767.

Kirchner, D.L., Gurnett, D.A., Safaeinili, A., Morgan, D.D., Huff, R.L., Plaut, J.J., Picardi, G., 2006. Radar sounding observations of the nightside Martian ionosphere. Geophys. Res. Abs. 8, 05224. abstract.

Kirchner, D.L., Gurnett, D.A., Winningham, J.D., Safaeinili, A., Plaut, J.J., Picardi, G., 2007. Auroral ionization patches on the nightside of Mars. Geophys. Res. Abs. 9, 04627. abstract.

Krymskii, A.M., Breus, T.K., Ness, N.F., Acuña, M.H., Connerney, J.E.P., Crider, D.H., Mitchell, D.L., Bauer, S.J., 2002. Structure of the magnetic field fluxes connected with crustal magnetization and topside ionosphere at Mars. J. Geophys. Res. 107, 1245.

Leblanc, F., and 14 colleagues 2008. Observations of aurorae by SPICAM ultraviolet spectrograph on board Mars Express: Simultaneous ASPERA-3 and MARSIS measurements. J. Geophys. Res. 113, A08311.

Liu, W., Victor, G.A., 1994. Electron energy deposition in carbon monoxide gas. Ap. J. 435, 909–919.

Lummerzheim, D., Lilensten, J., 1994. Electron transport and energy degradation in the ionosphere: Evaluation of the numerical solution, comparison with laboratory experiments and auroral observations. Ann. Geophys. 12, 1039–1051.

Lundin, R., and 22 colleagues 2006a. Plasma acceleration above Martian magnetic anomalies. Sci ence 311, 980-983.

Lundin, R., and 27 colleagues 2006b. Auroral plasma acceleration above Martian magnetic anomalies. Space Sci. Rev. 126, 333-354.

McDunn, T., Bougher, S. W., Murphy, J., Smith, M. D., Forget, F., Montmessin, F., Bertaux, J.-L. 2008. Simulating the density and thermal structure of the middle atmosphere (~70–130 km) of Mars using the MGCM-MTGCM: A comparison with MEX-SPICAM observations, Icarus, submitted.

Mendillo, M., Pi, X., Smith, S., Martinis, C., Wilson, J., Hinson, D., 2004. Ionospheric effects upon a satellite navigation system at Mars. Radio Sci. 39, RS2028.

Mitchell, D.L., Lin, R.P., Mazelle, C., Rème, H., Cloutier, P.A., Connerney, J.E.P., Acuña, M.H., Ness, N.F., 2001. Probing Mars' crustal magnetic field and ionosphere with the MGS Electron Reflectometer. J. Geophys. Res. 106, 23419–23427.

Mouginot, J., Kofman, W., Safaeinili, A., Herique, A., 2008. Correction of the ionospheric distortion on the MARSIS surface sounding echoes. Planet. Space Sci. 57, 917–926.

Newell, P.T., Greenwald, R.A., Ruohoniemi, J.M., 2001. The role of the ionosphere and aurora in space weather. Rev. Geophys. 39, 137–150.

Safaeinili, A., Kofman, W., Mouginot, J., Gim, Y., Herique, A., Ivanov, A.B., Plaut, J.J., Picardi, G., 2007. Estimation of the total electron content of the Martian ionosphere using radar sounder surface echoes. Geophys. Res. Lett. 34, L23204.

Sheehan, C.H., St.-Maurice, J.P., 2004. Dissociative recombination of $N_2^+, O_2^+$, and $NO^+$: Rate coefficients for ground state and vibrationally excited ions. J. Geophys. Res. 109, A03302.

Withers, P., Mendillo, M., Rishbeth, H., Hinson, D.P., Arkani-Hamed, J., 2005. Ionospheric characteristics above Martian crustal magnetic anomalies. Geophys. Res. Lett. 32, L16204.